Supplementary Information

Secondary Metal Ion-induced Electrochemical Reduction of U(VI) to U(IV) Solids

Xiaolu Liu,[1,3] Yinghui Xie,[1] Mengjie Hao,[1] Yang Li,[1] Zhongshan Chen,[1] Hui Yang,[1]* Geoffrey I. N. Waterhouse,[2] Xiangke Wang,[1]* and Shengqian Ma[3]*

[1] College of Environmental Science and Engineering, North China Electric Power University, Beijing 102206, P.R. China;

[2] School of Chemical Sciences, The University of Auckland, Auckland 1142, New Zealand;

[3] Department of Chemistry, University of North Texas, Denton, Texas 76201, United States;

Email: h.yang@ncepu.edu.cn (H.Y.); xkwang@ncepu.edu.cn (X.W.); shengqian.ma@unt.edu (S.M.)

Materials characterization

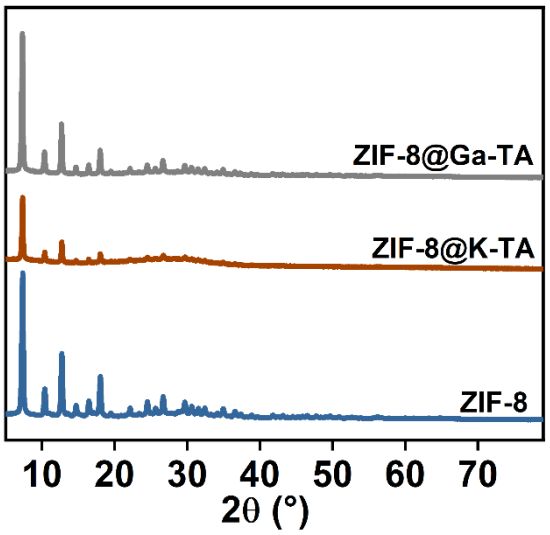

Supplementary Figure 1. PXRD patterns for ZIF-8, ZIF-8@K-TA, and ZIF-8@Ga-TA.

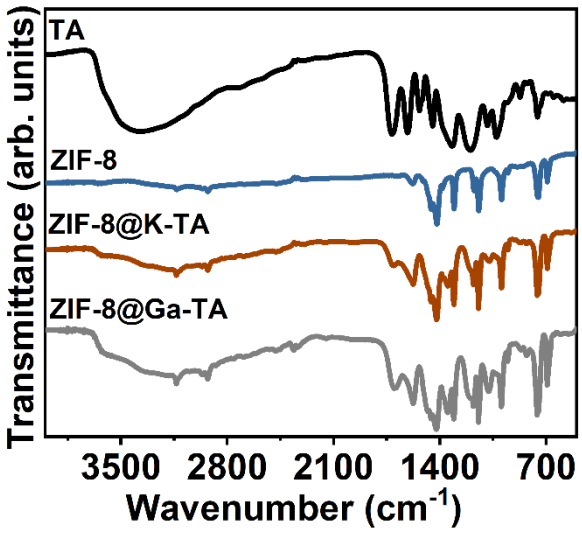

Supplementary Figure 2. FT-IR spectra for TA, ZIF-8, ZIF-8@K-TA, and ZIF-8@Ga-TA.

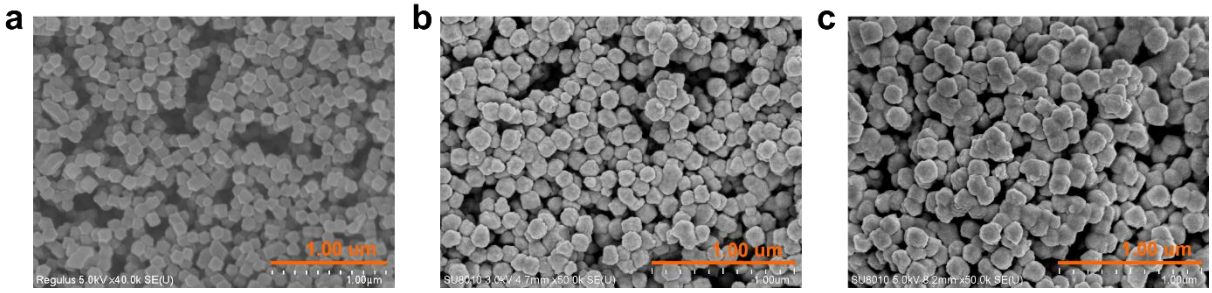

Supplementary Figure 3. SEM images for **a** ZIF-8, **b** ZIF-8@K-TA, and **c** ZIF-8@Ga-TA.

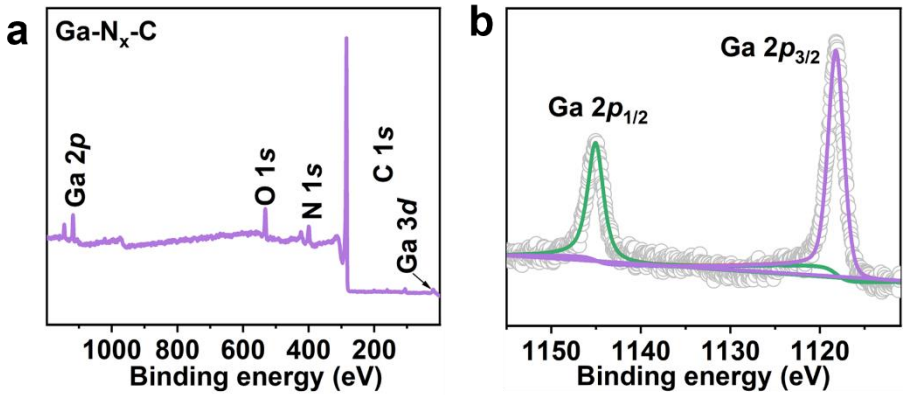

Supplementary Figure 4. a XPS survey spectrum and **b** Ga *2p* spectrum for Ga-N_x-C (right).

Supplementary Table 1. Uranium valence states in solid products produced in previous electrochemical uranium extraction studies.

Generated product	Condition	Reference
$(U(VI)O_2)O_2 \cdot 2H_2O$	Ambient conditions	1
$(U(VI)O_2)O_2 \cdot 2H_2O$	Ambient conditions	2
$U(VI)O_2(HO)_2$	Ambient conditions	3
$Na_2O(U(VI)O_3 \cdot H_2O)_x$	Ambient conditions	4
$U(VI)O_3/U_3O_8$	Ambient conditions	5
$Na_2O(U(VI)O_3 \cdot H_2O)_x$	Ambient conditions	6
$U(VI)O_3$	Ambient conditions	7
$Na_2O(U(VI)O_3 \cdot H_2O)_x$	Ambient conditions	8
$U(IV)O_2$/ $M_xU(IV)_yO_2$	Ambient conditions	This work

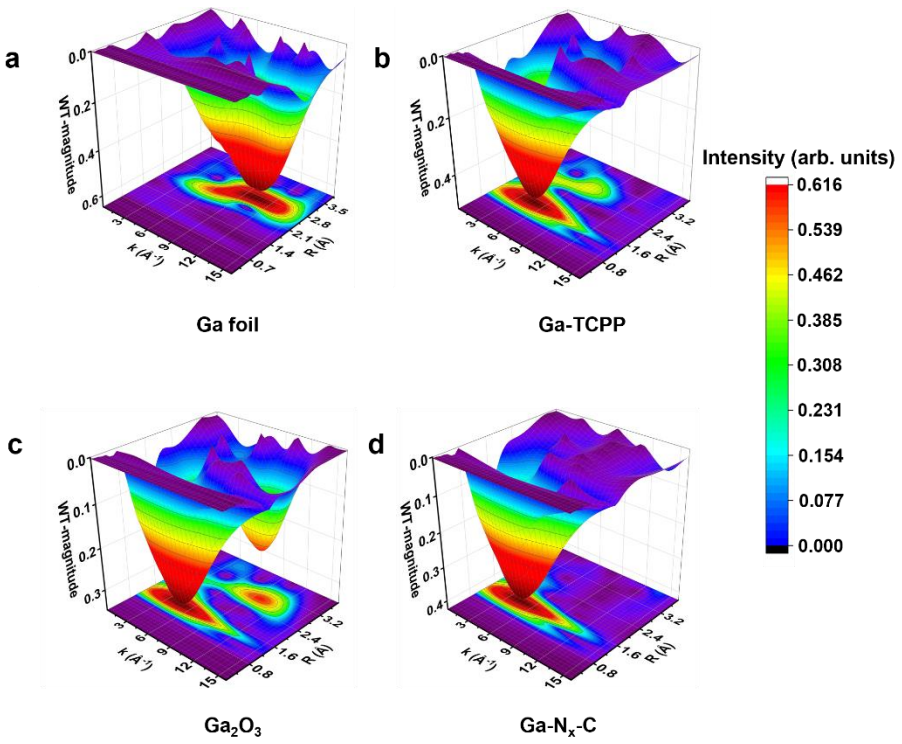

Supplementary Figure 5. Wavelet transform (WT) EXAFS plots for **a** Ga foil, **b** Ga-TCPP, **c** Ga_2O_3, and **d** Ga-N_x-C.

Supplementary Table 2. Summary of Ga K-edge EXAFS curve fitting parameters for Ga-N_x-C.

Sample	Path	R (Å)	CN	σ^2 (Å^2)	ΔE (eV)	R-factor
Ga-N_x-C	Ga-N	1.93836	4.132	0.00738	-0.777	0.0107696

R, distance between absorber and backscattering atoms; CN, coordination number; σ^2, Debye-Waller factor to account for both thermal and structural disorders; ΔE, inner potential correction; R-factor, indicates the goodness of the fit.

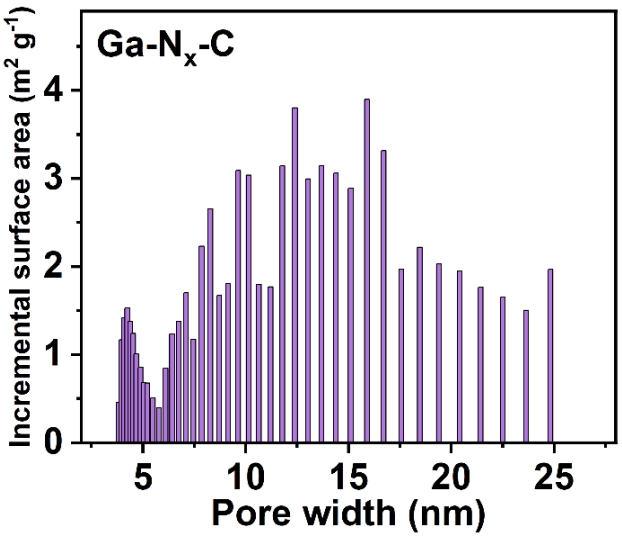

Supplementary Figure 6. Pore size distribution for Ga-N_x-C calculated using a NLDFT method from N_2 physisorption isotherms collected at 77 K.

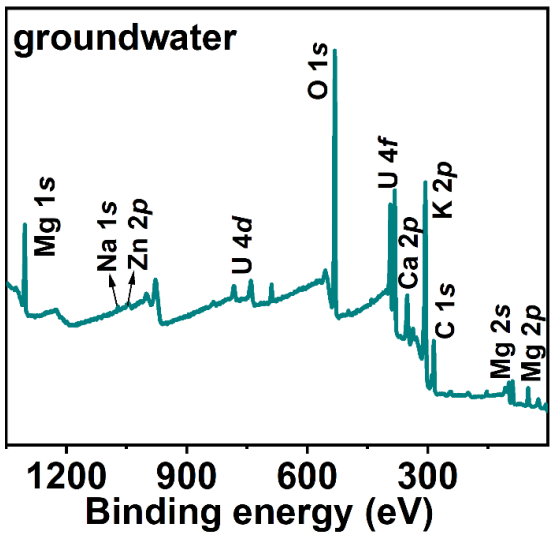

Supplementary Figure 7. XPS survey spectrum for the pale yellow product generated through electrocatalysis on Ga-N_x-C in ~20 ppm uranium-spiked groundwater.

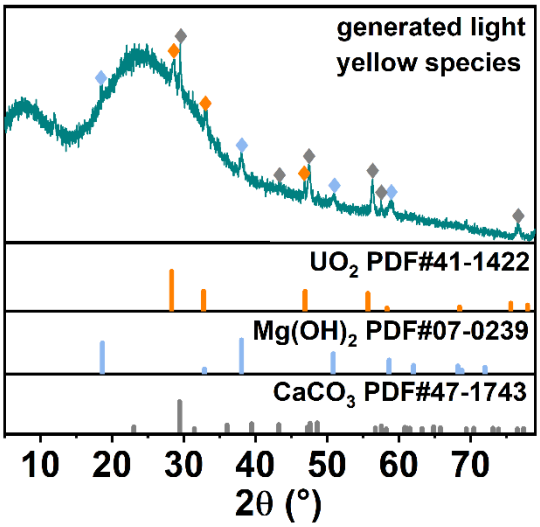

Supplementary Figure 8. PXRD patterns for the pale yellow product formed through electrocatalysis in ~50 ppm uranium-spiked groundwater.

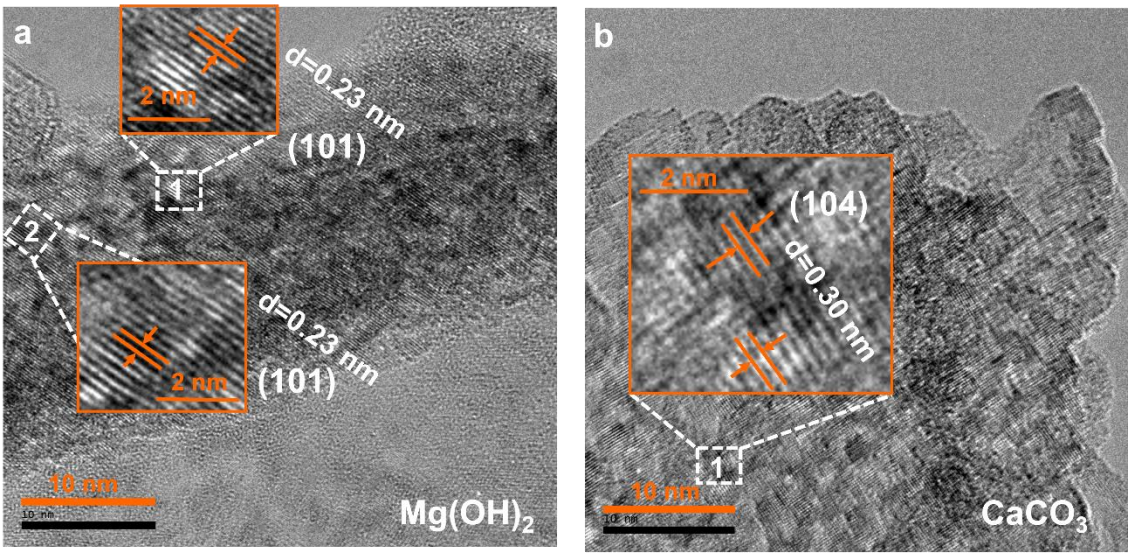

Supplementary Figure 9. HRTEM images of **a** $Mg(OH)_2$ and **b** $CaCO_3$ products generated through electrocatalysis on Ga-N_x-C in ~20 ppm uranium-spiked groundwater (inset: expanded view showing the lattice spacing.).

Supplementary Figure 10. Photograph of ~20 ppm uranium-spiked deionized water solution after 24 h of extraction using Ga-N_x-C. No solid product or other solid precipitate formed in the absence of other metal ions.

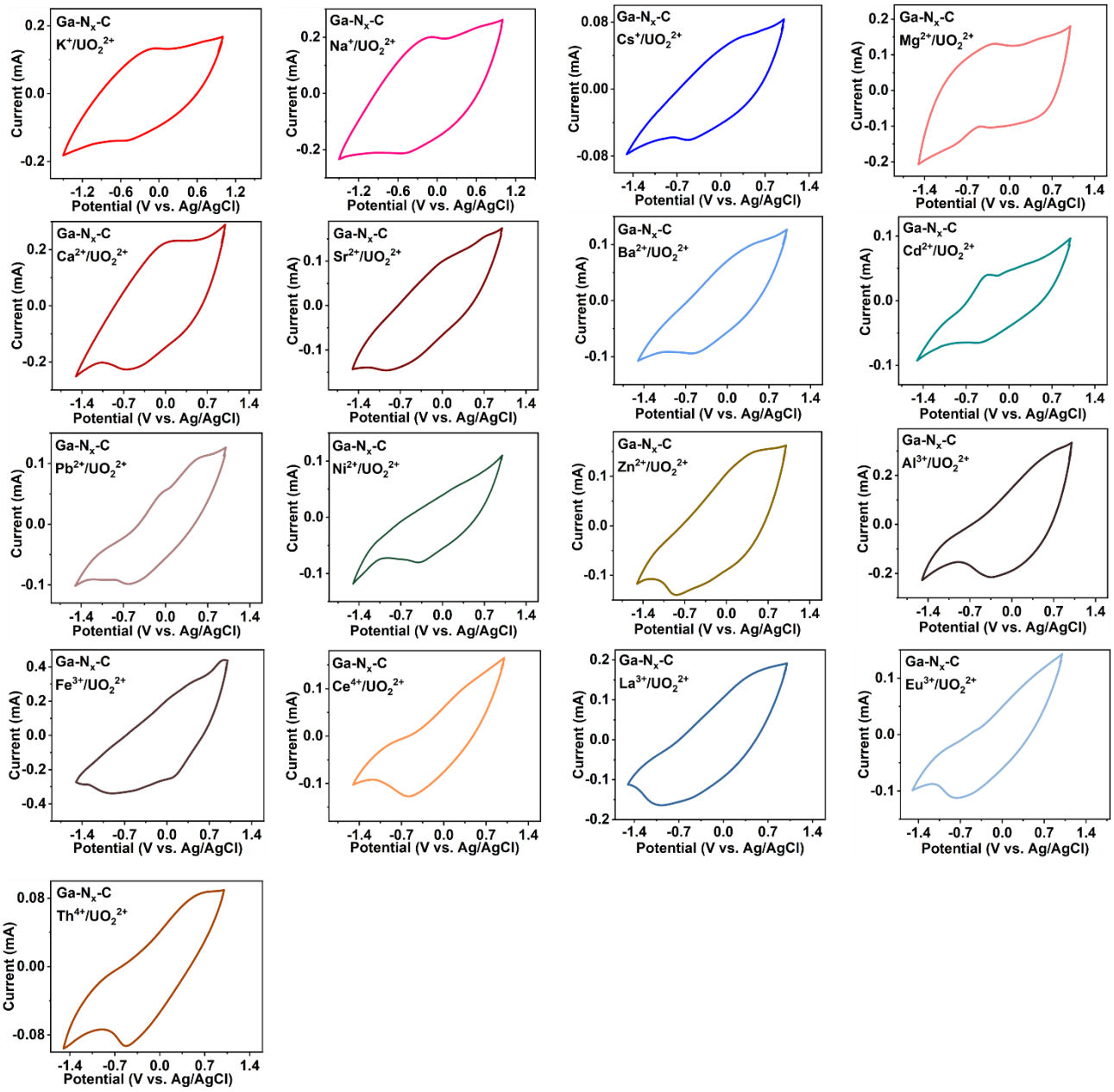

Supplementary Figure 11. Cyclic voltammograms of Ga-N_x-C/carbon felt in K^+/UO_2^{2+}, Na^+/UO_2^{2+}, Cs^+/UO_2^{2+}, Mg^{2+}/UO_2^{2+}, Ca^{2+}/UO_2^{2+}, Sr^{2+}/UO_2^{2+}, Ba^{2+}/UO_2^{2+}, Cd^{2+}/UO_2^{2+}, Pb^{2+}/UO_2^{2+}, Ni^{2+}/UO_2^{2+}, Zn^{2+}/UO_2^{2+}, Al^{3+}/UO_2^{2+}, Fe^{3+}/UO_2^{2+}, Ce^{4+}/UO_2^{2+}, La^{3+}/UO_2^{2+}, Eu^{3+}/UO_2^{2+}, and Th^{4+}/UO_2^{2+} aqueous solutions. The secondary metal concentrations were ~500 ppm, whilst the UO_2^{2+} concentration was also ~500 ppm.

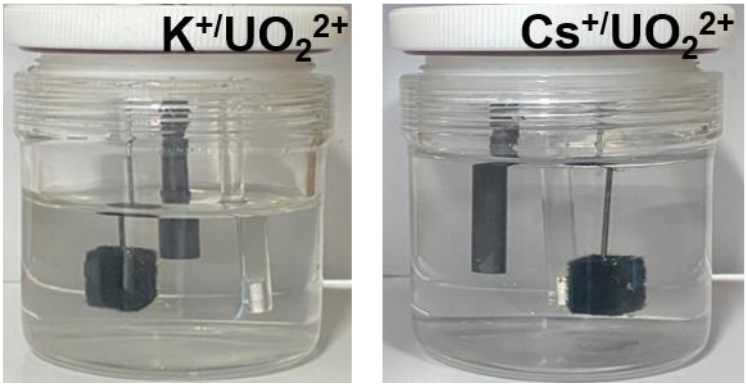

Supplementary Figure 12. Photographs of ~100 ppm uranium-spiked potassium nitrate solution (left) and uranium-spiked cesium nitrate solution (right) after 24 h of extraction using Ga-N_x-C. No solid product or other solid precipitate formed in the presence of K^+ or Cs^+.

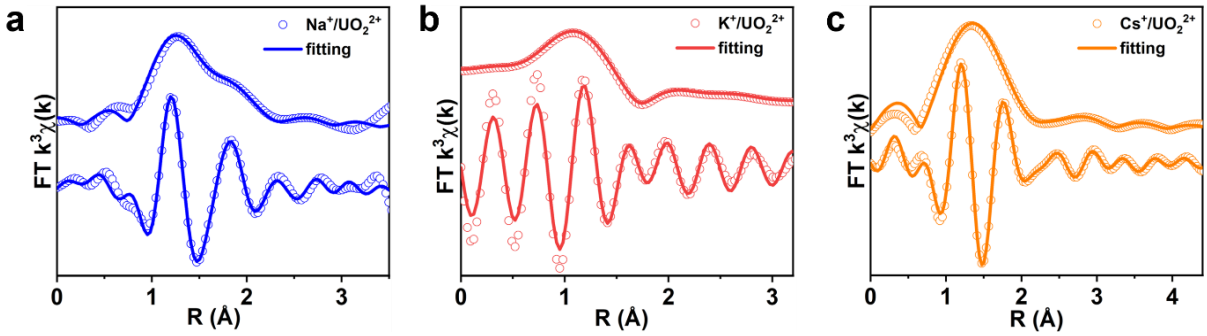

Supplementary Figure 13. Uranium L_3-edge EXAFS fitting curves for Ga-N_x-C after uranium extraction from aqueous solutions in presence of **a** Na^+/UO_2^{2+}, **b** K^+/UO_2^{2+}, and **c** Cs^+/UO_2^{2+}.

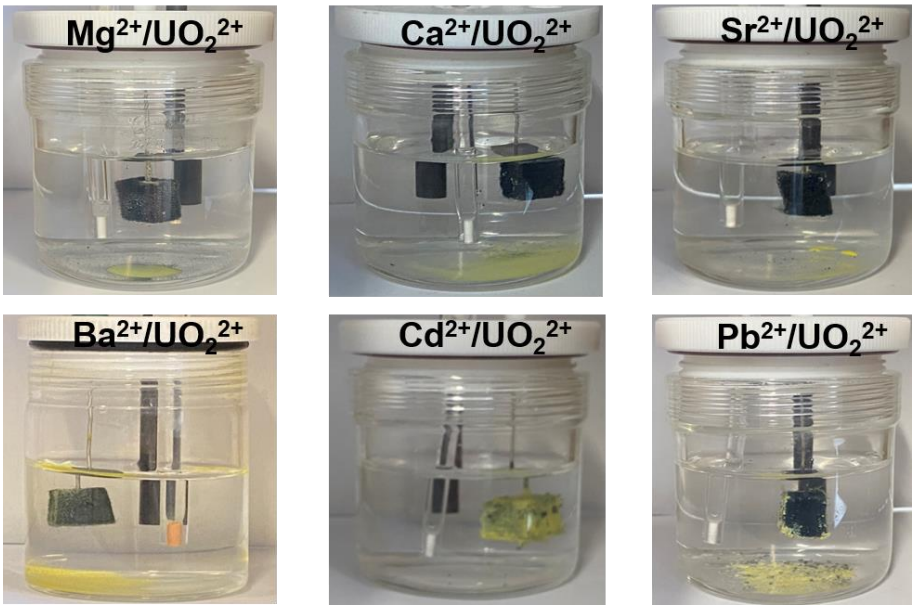

Supplementary Figure 14. Photographs of ~100 ppm uranium-spiked Mg^{2+}, Ca^{2+}, Sr^{2+}, Ba^{2+}, Cd^{2+}, and Pb^{2+} ions solutions after 24 h of extraction using Ga-N_x-C. Yellow solid products formed in the presence each of these secondary metal ions.

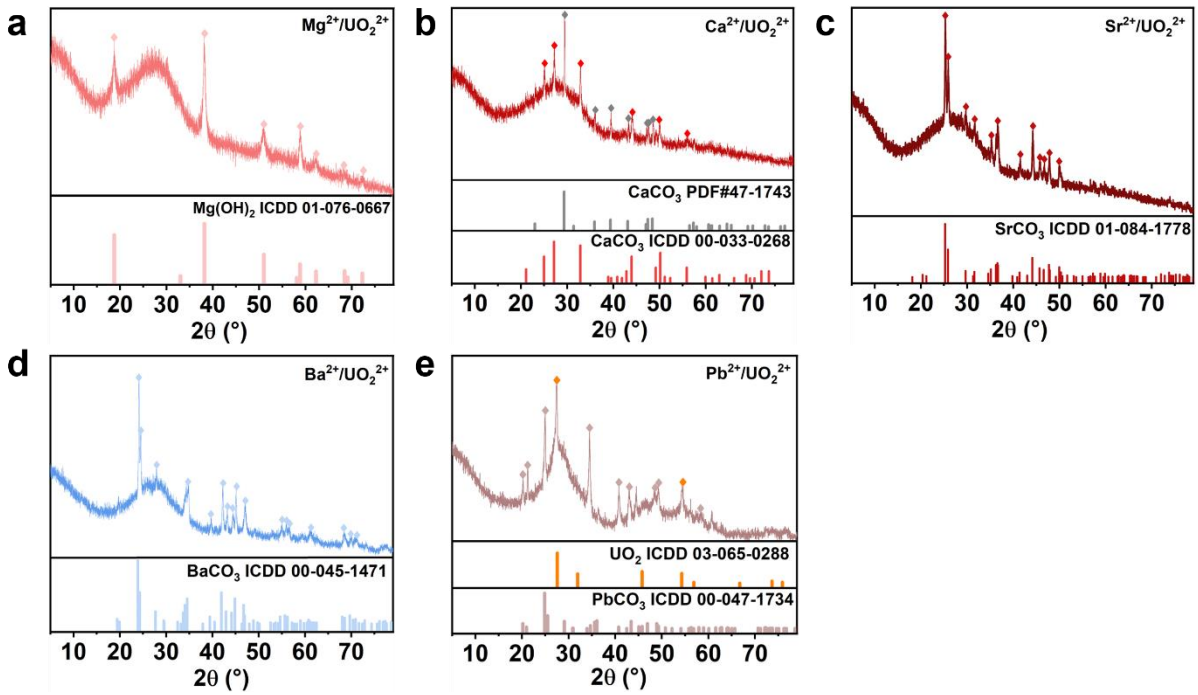

Supplementary Figure 15. PXRD patterns of electrocatalytically-generated solids formed in ~100 ppm uranium spiked **a** Mg^{2+}, **b** Ca^{2+}, **c** Sr^{2+}, **d** Ba^{2+}, and **e** Pb^{2+} ions solutions after 24 h of extraction using Ga-N_x-C.

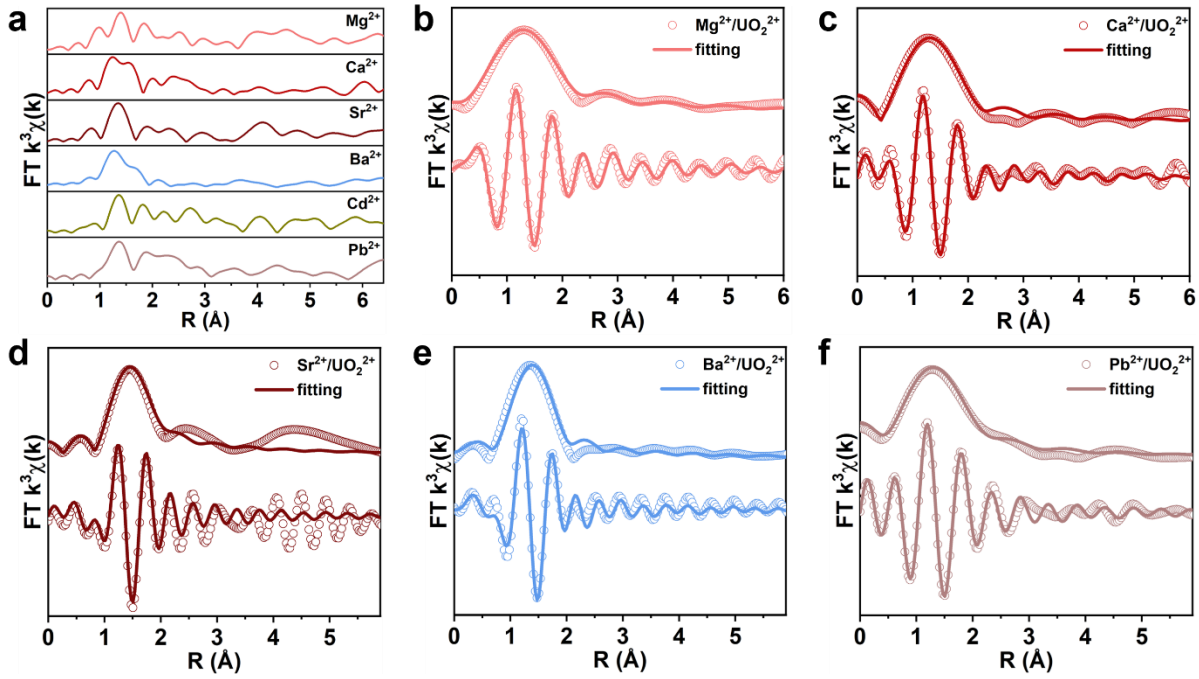

Supplementary Figure 16. a Uranium L_3-edge EXAFS and corresponding fitting curves of electrocatalytically-generated solids from uranium extraction in the presence of **b** Mg^{2+}, **c** Ca^{2+}, **d** Sr^{2+}, **e** Ba^{2+}, and **f** Pb^{2+}ions.

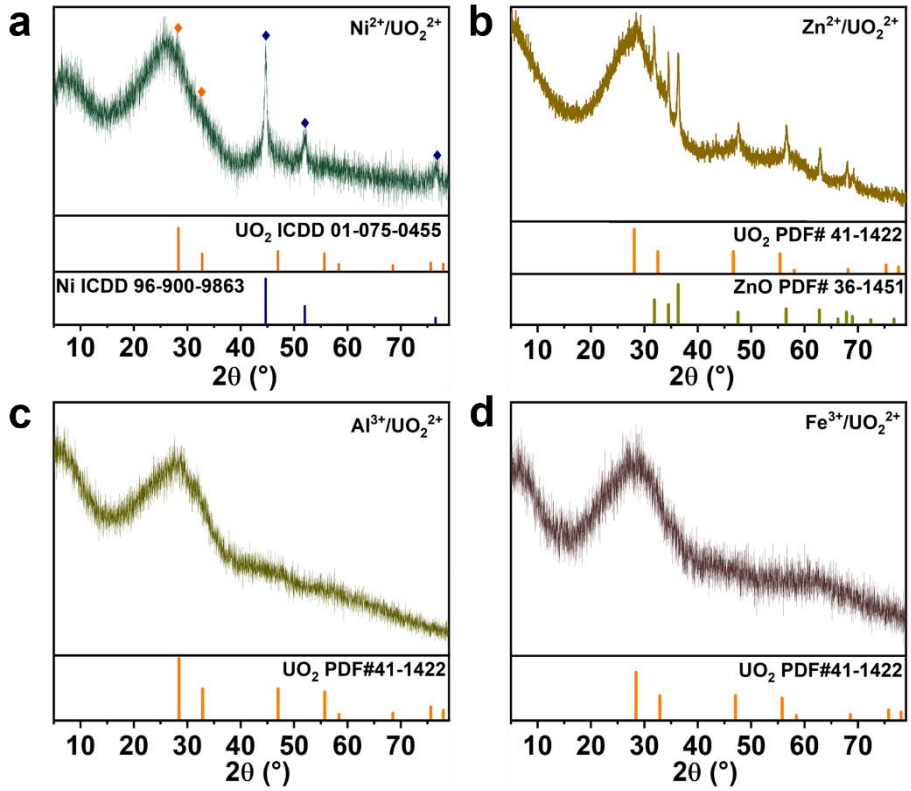

Supplementary Figure 17. PXRD patterns of electrocatalytically-generated solids formed in ~100 ppm uranium spiked **a** Ni^{2+}, **b** Zn^{2+}, **c** Al^{3+}, and **d** Fe^{3+} ions solutions after 24 h of extraction using Ga-N_x-C.

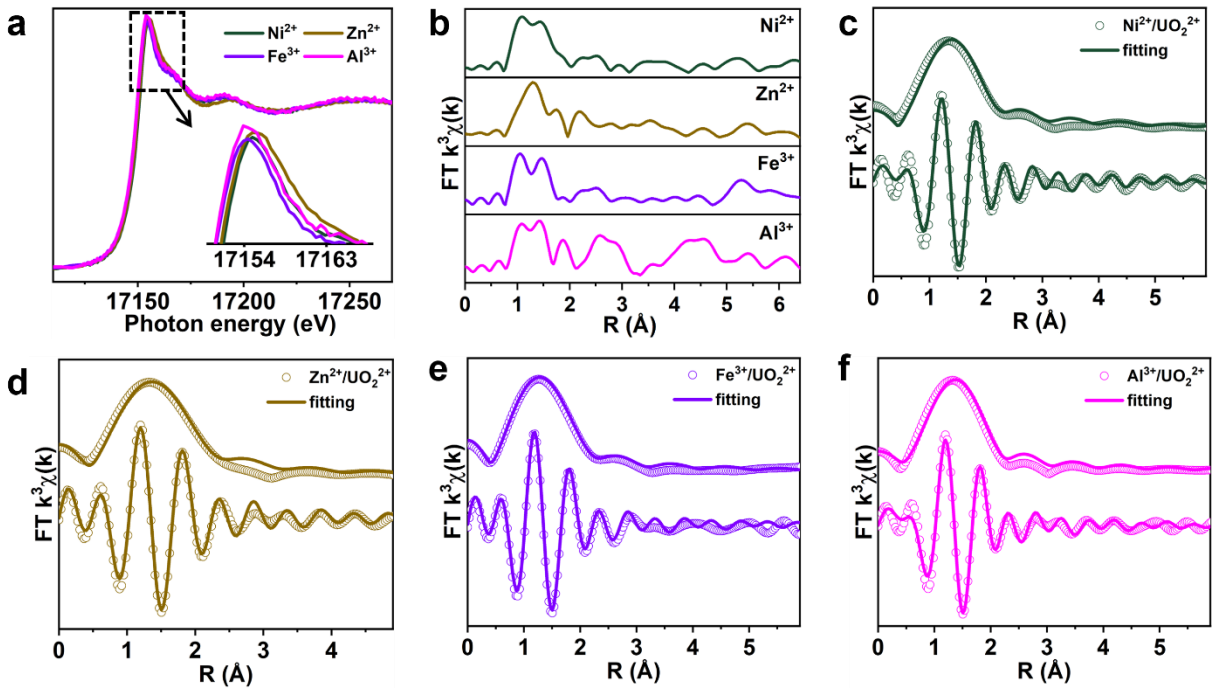

Supplementary Figure 18. a Uranium L_3-edge XANES (inset: expanded view showing the U valence states.), **b** EXAFS and corresponding fitting curves of electrocatalytically-generated solids from uranium extraction in the presence of **c** Ni^{2+}, **d** Zn^{2+}, **e** Fe^{3+}, or **f** Al^{3+} ions.

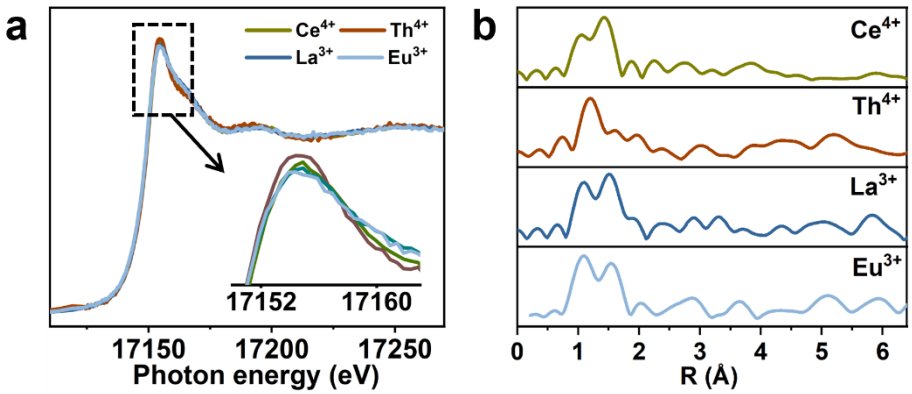

Supplementary Figure 19. a Uranium L_3-edge XANES (inset: expanded view showing the U valence states.) and **b** EXAFS curves for solids generated during uranium extraction from aqueous solutions in presence of Ce^{4+}, Th^{4+}, La^{3+}, or Eu^{3+} ions.

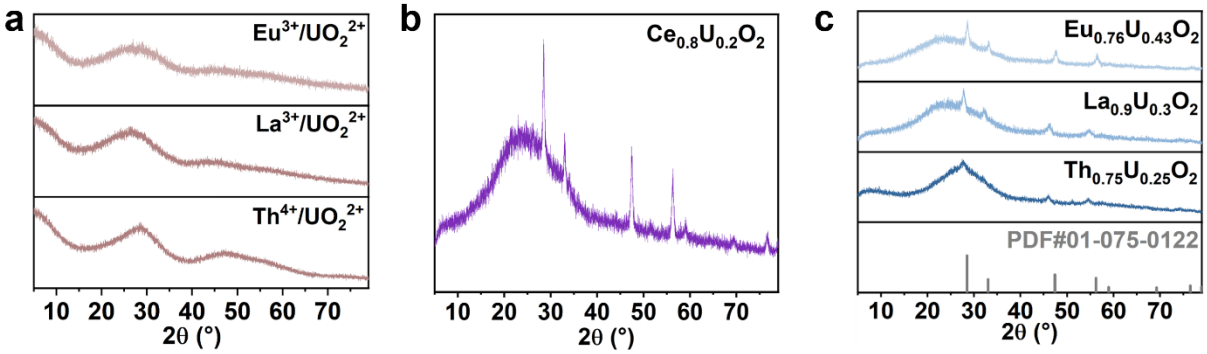

Supplementary Figure 20. a PXRD patterns of electrocatalytically-generated solids formed in ~100 ppm uranium-spiked Eu^{3+}, La^{3+}, and Th^{4+} ions solutions after 24 h of extraction using Ga-N_x-C. **b** PXRD pattern of electrocatalytically-generated $Ce_{0.8}U_{0.2}O_2$ after annealing in air. **c** PXRD patterns of electrocatalytically-generated solids formed in ~100 ppm uranium-spiked Eu^{3+}, La^{3+}, and Th^{4+} ions solutions after annealing in air (showing the formation of crystalline bimetallic oxides, PDF standard card from the International Centre for Diffraction Data-ICDD).

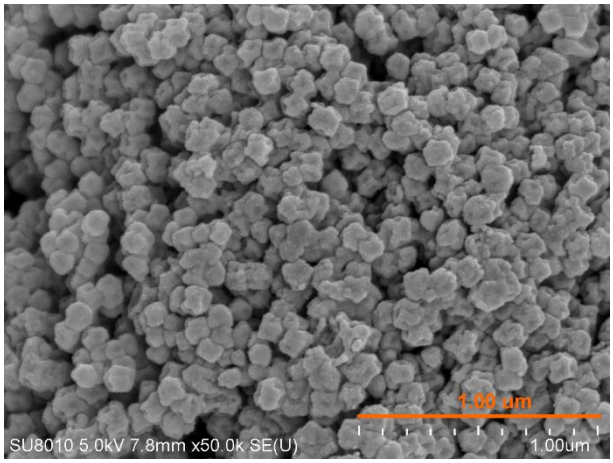

Supplementary Figure 21. SEM image of Ga-N_x-C after electrocatalysis under LMW conditions.

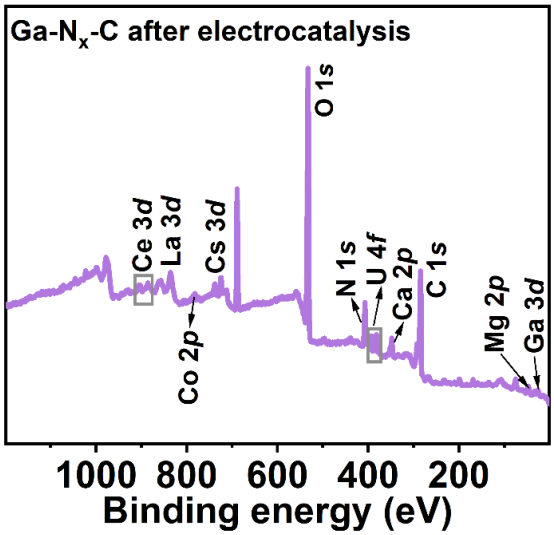

Supplementary Figure 22. XPS survey spectrum of Ga-N_x-C after electrocatalysis in a simulated LMW solution.

Supplementary Methods

Molecular dynamics (MD) simulations

Molecular dynamic (MD) simulations were applied to investigate the assembly, distribution and diffusion of anions and cations in aqueous solution. Four kinds of solution systems consisting of different numbers of components were constructed in cubic simulation boxes. All MD simulations were carried out by Forcite module with universal force field (UFF)[9] in Materials Studio (MS) 2020. The partial charges for each atom were assigned by the QEq method. Van der Waals and Coulombic interactions were considered by atom based and Ewald methods, respectively, with a cut-off value of 15.5 Å. Equations of motion were integrated with a time step of 1 fs. After energy minimization, each system was fully relaxed under periodic boundary conditions for 500 ps in the NVT (T = 298.0 K) ensemble using the Nose thermostat, which was long enough for system temperature, potential and total energy to be stable. The dynamic trajectories of the last 250 ps were outputted at an interval of 5 ps for radial distribution function (RDF), mean square root (MSD) and relative concentration distribution analysis.

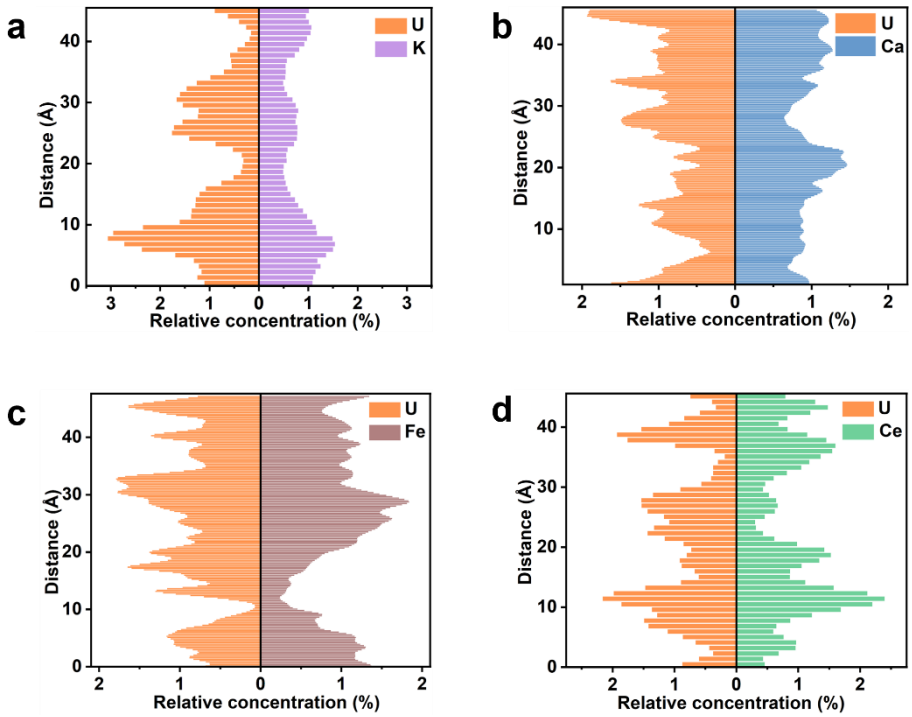

Supplementary Figure 23. Relative concentration of **a** U(IV)/K^+, **b** U(IV)/Ca^{2+}, **c** U(IV)/Fe^{3+}, and **d** U(IV)/Ce^{4+} calculated by molecular dynamics simulations.

Supplementary References

1. Liu, C. et al.. A half-wave rectified alternating current electrochemical method for uranium extraction from seawater. *Nat. Energy* **2**, 17007 (2017).
2. Ye, Y. et al. Spontaneous electrochemical uranium extraction from wastewater with net electrical energy production. *Nat. Water* **1**, 887-898 (2023).
3. Wang, C. et al. Uranium in situ electrolytic deposition with a reusable functional graphene-foam electrode. *Adv. Mater.* **33**, 2102633 (2021).
4. Yang, H. et al. Functionalized iron-nitrogen-carbon electrocatalyst provides a reversible electron transfer platform for efficient uranium extraction from seawater. *Adv. Mater.* **33**, 2106621 (2021).
5. Wang, Y. et al. Electrochemical-mediated regenerable Fe^{II} active sites for efficient uranium extraction at ultra-low cell voltage. *Angew. Chem. Int. Ed.* **62**, e202217601 (2023).
6. Liu, X. et al. Highly efficient electrocatalytic uranium extraction from seawater over an amidoxime-functionalized In-N-C catalyst. *Adv. Sci.* **9**, 2201735 (2022).
7. Wang, Y. et al. Strengthening Fe(II)/Fe(III) dynamic cycling by surface sulfation to achieve efficient electrochemical uranium extraction at ultralow cell voltage. *Environ. Sci. Technol.* **57**, 13258-13266 (2023).
8. Chen, D. Y. et al. Self-standing porous aromatic framework electrodes for efficient electrochemical uranium extraction. *ACS Cent. Sci.* **9**, 2326-2332 (2023).
9. Rappe, A. K., Casewit, C. J., Colwell, K. S., Goddard Iii, W. A., & Skiff, W. M. UFF, A full periodic table force field for molecular mechanics and molecular dynamics simulations. *J. Am. Chem. Soc.* **114**, 10024-10035 (1992).